Nanoscale

PAPER

Check for updates

Cite this: *Nanoscale*, 2017, **9**, 11480

Thermal rectification at the bimaterial nanocontact interface†

Zhen-Qiang Ye and Bing-Yang Cao *

Received 16th April 2017,
Accepted 13th July 2017

DOI: 10.1039/c7nr02696j

rsc.li/nanoscale

Thermal rectification can help develop modern thermal manipulation devices but has been rarely engineered. Here, we validated the nanoscale bimaterial interface-induced thermal rectification experimentally for the first time and investigated its underlying mechanism *via* molecular dynamics simulations. The thermal diode consists of polyamide (PA) and silicon (Si) nanowires in contact with each other. The thermal rectification ratio measured by a high-precision nanoscale experiment reached 4% with an uncertainty of <1%. The temperature has little influence on the ratio, while the decrease in contact length or increase in temperature differences can increase the ratio. The molecular dynamics simulations further confirmed the thermal rectification in the PA/Si nanowires. We found that the localized modes generally gather on the edge, and the higher extent of phonon localization is responsible for the lower thermal conductance in the thermal rectification. Our findings not only have guiding significance, but can also promote the development of interface-based solid-state thermal diodes.

1. Introduction

Devices with more flexible controls in heat flux, especially at the nanoscale, have drawn increasing attention in recent years.[1,2] Although thermal science has a longer history than electrics, its development lags far behind the latter in many aspects.[3,4] For example, electric diodes with the ability for current rectification are widely used in daily life, but there is no mature analog in the thermal field. Thermal rectification is the counterpart of the electric diode for heat conduction and was first discovered in 1936.[5] A device with thermal rectification effects is called a thermal rectifier or a thermal diode whose thermal conductance along a specific direction is different from that in the reverse direction.[6] A thermal rectifier provides a fundamental element in some novel schemes of "thermal circuits" including as a thermal transistor,[4] thermal memory[7] or thermal modulation.[8] This suggests that the "thermal computer" used in thermal control and management may be realized in the future. It is of both scientific and applied significance to design a mature product with thermal rectification. Thus, thermal rectification has aroused increasing concern in recent years.[9–30]

Pioneering theoretical studies of one-dimensional nonlinear lattices allow the study of nanoscale thermal rectification.[7–11] Li *et al.* put forward a theoretical model of thermal memory[7] and thermal gates[11] based on the thermal rectification effects in one-dimensional nonlinear lattices. The asymmetry and non-linearity factors are believed to be the two dominant and indispensable factors in nanoscale thermal rectification systems.[12] Hence, numerous proposals based on asymmetry and non-linearity including asymmetric carbon nanotubes,[6] trapezoidal graphene nanoribbons[13] and graded nanowires have emerged in past years.[15] These are collectively known as phonon-based thermal rectifiers. Besides phonon-based devices, there are also electron-based[17] and photon-based[23,24] counterparts. This dramatic breakthrough is due to the seminal experimental research by Chang *et al.*,[16] in which they designed a solid-state nanoscale thermal rectifier. Although its thermal rectification factor remains very limited, it could be used to design a real thermal diode. After that, some passive solid-state thermal rectifiers experimentally achieved appreciable thermal rectification ratios, such as phase change thermal rectification[31–33] and shape memory alloy thermal rectification.[21] However, these solid-state nanoscale thermal rectifiers need a complex external source, which makes them very inconvenient. Most existing proposals have very complex structures including high-precision devices,[16,23,34] or external sources to drive.[21,31,35] Easily prepared thermal rectifiers are highly desired to direct the development of thermal diodes.

Lately, theoretical studies have indicated that the interfacial effect in a bimaterial system can also lead to thermal

Key Laboratory for Thermal Science and Power Engineering of Ministry of Education, Department of Engineering Mechanics, Tsinghua University, Beijing 100084, P. R. China. E-mail: caoby@tsinghua.edu.cn; Fax: +86-10-6279-4531; Tel: +86-10-6279-4531

†Electronic supplementary information (ESI) available. See DOI: 10.1039/c7nr02696j

This journal is © The Royal Society of Chemistry 2017

rectification.[25–29,22,36–40] Bimaterials usually consist of two quite different materials such as fluid/solid,[22] metal/dielectric,[38] and organic/inorganic (crystal/polymer).[29,30] Apparently, the thermal rectifier of the bimaterial system is much easier to fabricate than that based on changing the structure of a single material. Thus, the interface-induced thermal diode can be realized as a mainstream idea of a thermal diode in the future. However, to this day, no experimental proof can validate the interface-induced thermal rectification and its physical mechanism remains ambiguous at the nanoscale. Currently, there are three main approaches to interpret the thermal rectification mechanisms: mismatch of the power spectra of two nanostructures,[15] temperature-dependent thermal properties,[29] and different extents of phonon localization.[6] These factors may be coupled with each other or work separately. The physical essence of interface-induced thermal rectification is still an open question.

Here, we demonstrate that interface-induced thermal rectification can be realized by sophisticated experiments and molecular dynamics (MD) simulations. Moreover, we propose a brand new mechanism to guide the design of interface-induced thermal rectifiers. To successfully carry out these experiments, two difficulties must be overcome. The first is to prepare the samples. The experiments should be conducted at the nanoscale because the interfacial resistance dominates the heat conductance of the entire system. Considering both the feasibility and application value, we established an organic/inorganic system consisting of a silicon (Si) nanowire and a polyamide (PA) nanofiber. Si is the most important semiconducting material in nanoelectronics, and PA is widely known as nylon—a very popular organic material with advantageous mechanical properties. More importantly, both of them are easy to produce. The second difficulty lies in the measurement of the thermal rectification ratio. Our platform has a very high resolution of heat flux, 10^{-13} W K^{-1}, which has been used in previous nanoscale experiments by Chen *et al.*[41] The radiation and convection loss can be ignored so that the uncertainty is reduced to <1%. The MD simulations are then used to reveal the underlying mechanism. We propose and validate an easy but effective way to achieve interface-induced thermal rectification. This is a promising approach for the design of thermal diodes.

2. Experimental study

2.1 Experimental method

We created a high-resolution experiment to measure the thermal conductance on a sensitive micro-device platform.[41] The micro-device consists of a heating beam and a sensing beam, both of which are made of SiN_x (the circuit diagrams are in the ESI Note 1†). The specimen is suspended between the two beams. The entire micro-device is placed in a high vacuum cryostat for eliminating the convection loss. The radiation heat loss is also negligible.[41] A 1-ω AC current is applied on the heating beam, and a DC current is applied on the sensing side. The heating power is a 2-ω signal so the temperature rise is a 2-ω signal as well. The resistance rise is proportional to the temperature rise. Combined with the current, we get 3-ω and 2-ω voltage changes at the heating beam and the sensing beam, respectively. This estimates their temperature rise to be ΔT_h and ΔT_s, respectively (see the ESI Note 1†). The heat flux in the sensing beam, Q_{beam}, and the thermal conductance of the beam, G_{beam}, are related as

$$Q_{beam} = G_{beam}(\Delta T_h - \Delta T_s). \quad (1)$$

Based on the heat balance analyses, the thermal conductance of the specimen, G, is

$$G = G_{beam}\frac{\Delta T_s}{(\Delta T_h - \Delta T_s)}. \quad (2)$$

Fig. 1 shows the SEM images of the PA/Si nanowire thermal rectifier suspended between two beams. The organic part of the rectifier is an aligned PA-11 nanofiber produced *via* electrospinning. PA is a widely used polymer material with high performance that is relatively easy to produce.[42] The inorganic side is a Si nanowire synthesized by the chemical vapor deposition growth method.[43] To avoid heat loss, the redundant part of the specimen should be removed *via* a focused ion beam (FIB), and the sample before FIB cutting is shown in the inset of Fig. 1a. The Si nanowire and the PA nanofiber have diameters of 140 nm and 580 nm, respectively, and both are fixed on the pads with platinum.

The thermal rectification ratio, η, is defined as

$$\eta = \frac{|G_{PS} - G_{SP}|}{G_{SP}} \times 100\%, \quad (3)$$

where G is the thermal conductance, 'PS' refers to the heat flux from PA to Si, and 'SP' is the reverse.

2.2 Experimental results and discussion

First, we focus on the influence of heat flux because previous analyses[29] suggest that heat flux has a significant influence on thermal rectification. In our experiments, the applied voltage

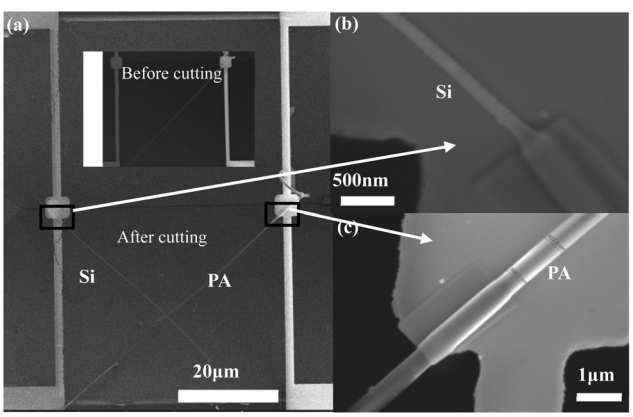

Fig. 1 SEM images of: (a) the entire thermal rectifier, and the inset is the sample before FIB cutting; (b) Si nanowire; and (c) PA-11.

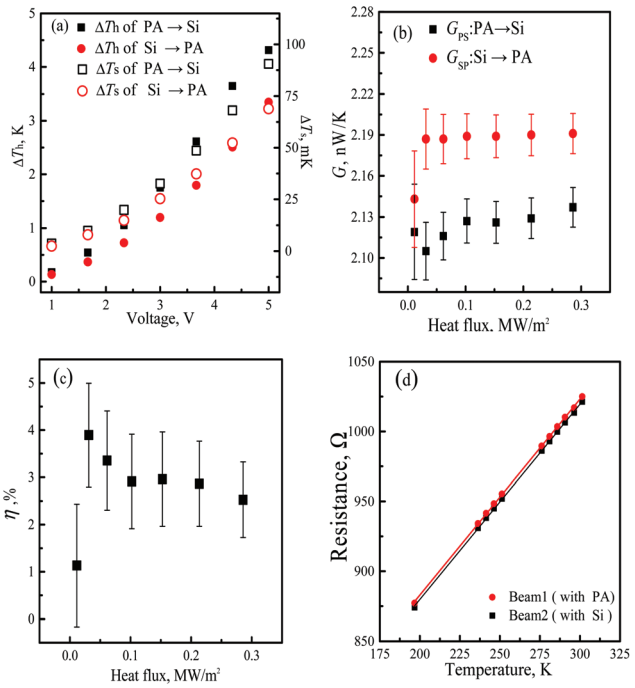

Fig. 2 (a) Temperature rise as a function of voltage; (b) thermal conductance: G_{PS} and G_{SP}; (c) thermal rectification ratio as a function of heat flux; and (d) temperature-dependent resistance of the two beams.

in the heating beam ranges from 1 V to 5 V. Fig. 2a shows the temperature rise of the heating beam, ΔT_h, and the sensing beam, ΔT_s, at the room temperature environment. The maximum ΔT_h and ΔT_s are about 4.3 K and 0.08 K, respectively, implying that the latter is almost two orders of magnitude less than the former. That is because the heat flux in the sensing beam is much lower than that in the heating beam. Fig. 2b shows the thermal conductance of the rectifier. Apparently, G_{SP} is always larger than G_{PS}, which verifies the existence of thermal rectification. We emphasize that the error mainly comes from the sensing side because ΔT_s is very subtle. A lower heat flux leads to a higher relative error, and the error in low heat flux measurements is relatively larger. It is estimated that the interface dominates in heat transfer. In the ESI, Fig. S7† shows that the thermal conductivity of a single PA fiber with a diameter of 870 nm is about 0.55 W (m K)$^{-1}$ at room temperature. Since the thermal conductivity of the PA fiber increases with a reducing diameter,[41] hence, the thermal conductivity of PA in Fig. 1 should be higher than 0.55 W (m K)$^{-1}$ at room temperature; in other words, the estimated thermal conductance should be higher than 5.58 nW K^{-1} ($\lambda\pi R^2/L$, $R \approx 400$ nm, $L \approx 50$ μm). However, for the first PA/Si sample, it is only 2.1 nW K^{-1} as shown in Fig. 2b. Hence, the interface plays an important role in heat transfer.

Fig. 2c shows the thermal rectification ratio as a function of heat flux at room temperature. Except for the first point, η is around 3%. We can check the temperature coefficient of resistance (TCR) when the asymmetry of the micro-device leads to pseudo-rectification . Fig. 2d shows that the TCRs of the two beams are nearly the same throughout the entire temperature range. This means that the two beams are nearly equivalent. The effect of the asymmetric micro-device can thus be excluded. In other words, the observed thermal rectification is probably due to the change in thermal properties of the specimen. This will be discussed in more detail below. In general, there is no significant relevance between the heat flux and the rectification performance according to Fig. 2c. This is due to the low heat flux. The high heat flux has been shown to have a significant impact on thermal rectification.[29] However, we cannot apply a very high heat flux for fear of damaging the specimen. The influence of the heat flux will be further studied *via* MD simulations.

Next, we investigated the temperature dependence of thermal rectification. Fig. 3a represents the thermal conductance of the rectifier at different temperatures. G_{SP}, *i.e.*, Si-to-PA, always has a higher thermal conductance. The thermal conductance reduces by about 40% as the temperature declines from 296.6 K to 96.8 K mainly due to the decrease in the PA thermal conductance. Fig. 3b shows that the thermal rectification ratio varies from 2.8% to 3.5%; so the temperature does not easily influence the thermal rectification ratio (uncertainty analyses are in the ESI Note 2†).

To further verify the rectification of this interface-induced rectifier, we checked another specimen consisting of PA and Si nanowires in contact with each other. We emphasize that the two specimens have a significant difference in contact area. Fig. 4a indicates that the second specimen has a visible deformation due to the internal stress after FIB cutting. Thus, the contact area is much larger than that of the first, which means the thermal contact resistance may be lower for the second specimen. Fig. 4b shows the thermal conductance and Fig. 4c shows the thermal rectification ratio. Similarly, the thermal conductance increases with increasing temperature, and the error bar is still acceptable. G_{SP} is always larger than G_{PS} under different temperatures, which agrees well with the first specimen. The thermal rectification ratio has a slight rise from 2.7% to 3.4% as the temperature drops from 296.5 K to 246.3 K. In short, both specimens have about a 3% thermal rectification ratio, and there is still no notable relevance between the thermal contact resistance and the thermal rectifi-

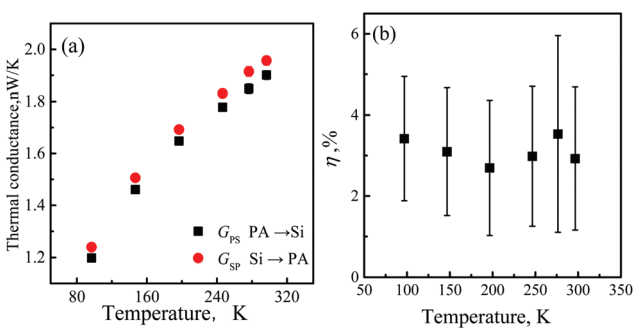

Fig. 3 Temperature-dependent (a) thermal conductance: G_{PS} and G_{SP}; and (b) thermal rectification ratio with error bars.

This journal is © The Royal Society of Chemistry 2017

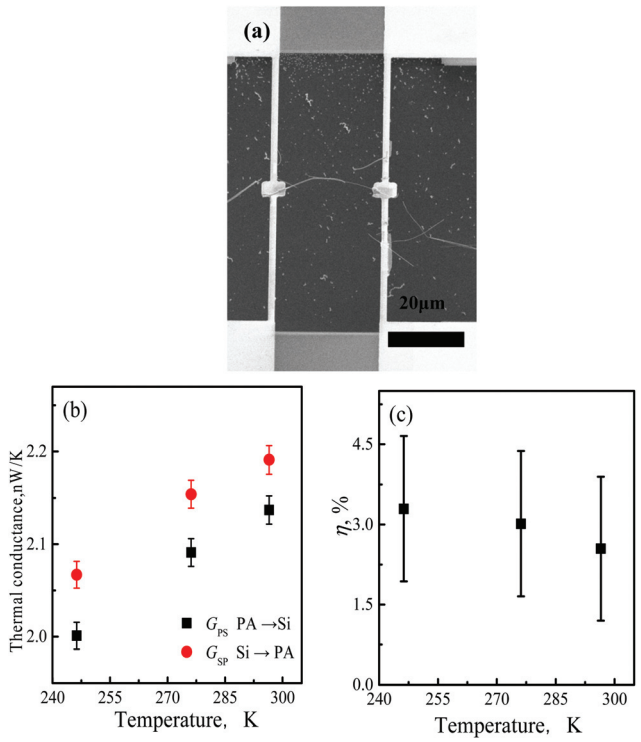

Fig. 4 (a) The second specimen after FIB cutting; (b) measured thermal conductance: G_{PS} and G_{SP}; and (c) thermal rectification ratio with error bars.

cation ratio in our experiments. Since the measurement uncertainty is about 1%, the difference between the two samples is concealed by the uncertainty.

Our experiments directly prove the existence of thermal rectification in the PA/Si nanowire interface. A similar thermal rectification ratio of about 3% is observed for both specimens. The experimental conditions are limited because we cannot apply a very high temperature gradient. Therefore, we cannot confirm that there is no obvious relevance of the thermal rectification ratio to temperature and heat flux current conditions. Hence, the following MD studies can conquer the limitations of the experiments, and help us reveal the underlying physical mechanism.

3. Molecular dynamics study

3.1 Simulation method

The MD simulation was performed *via* the LAMMPS package.[44] First, we generated stable polymer chains. The molecular formula of PA-11 is –[(NH–CO)–$(CH_2)_{11}$]–. Non-equilibrium MD (NEMD) simulations were used to calculate the thermal conductance of the PA/Si nanowires. The time step is 0.25 fs. The system is first relaxed in the NVT ensemble for 1 000 000 steps, then in the NEMD for another 5 000 000 steps. The X direction is a fixed boundary condition, and the Y and Z directions are free boundary conditions. The atoms on the ends are placed in the Nosé–Hoover thermostats[45] with temperatures T_H and T_L. The motion equations of the atoms in the thermostats are

$$\frac{d}{dt}p_i = F_i - \gamma p_i; \tag{4.1}$$

$$\frac{d}{dt}\gamma = \frac{1}{\tau^2}\left[\frac{T(t)}{T_0} - 1\right]; \tag{4.2}$$

$$T(t) = \frac{2}{3Nk_B}\sum_i \frac{{p_i}^2}{2m_i}. \tag{4.3}$$

Here, p_i, F_i and m_i are the momentum, force and mass of atom i, respectively. Term γ is the dynamic parameter, τ is the relaxation time of the thermostats, k_B is the Boltzmann constant, and N is the number of atoms in the thermostat. The heat flux applied to the thermostats is given by $Q = -3\gamma Nk_BT(t)$. The thermal conductance is deduced from Fourier's law: $G = Q/\Delta T$. In the MD simulations, the potential model for PA-11 is modeled by the modified OPLS force field[46,47] that is partly derived from the all-atom model of *N*-methylacetamide proposed by Caldwell *et al.*[47] The Stillinger–Weber potential[48] is used to generate the Si nanowire. The interaction between PA and Si is characterized by the van der Waals' force (the verification of the potential function is in the ESI Note 3†). It should be emphasized that Pal *et al.*[30] also investigated the thermal rectification between the crystal and polymer, but the interface interaction was defined by covalent bonds in their simulations. Hence, the mechanisms of the two cases are different. The schematic of the PA/Si nanowires is shown in Fig. 5a. The initial length of PA is 10 nm and is 8 nm for Si. The influence of size effect in the direction of heat flux is shown in the ESI Note 3.† The contact length of the PA and Si, L_{cross}, is set as 2 nm and 4 nm, respectively. Both of these have a diameter of about 1.5 nm. The temperature difference, ΔT, is set to 30 K, 60 K, 100 K, 150 K and 200 K.

It should be emphasized that the simulations are still different with the experiments, though we try our best to imitate the real situations. First, the size is different since the real size needs a too huge computation cost. Second, the nylon fiber structure is simplified to the multi-chain structure. The real structure is more complicated and amorphous. Third, the contact area in the experiment is not easy to be distinguished; so the interface in the simulations is simpler. Hence, the simulations may not capture some of the features observed in the experiments. Nevertheless, the calculations can provide an additional qualitative insight.

3.2 Simulation results and discussion

Fig. 5b shows the energy accumulation applied to the thermostats where ΔT = 100 K, and L_{cross} is set as 2 nm and 4 nm, respectively, to study its influence. The derivative of the energy accumulation is heat flux, *i.e.*, $Q = dE/dt$. Thus, the slope of the curves in Fig. 5b can reflect the intensity of the heat flux. We can deduce three main conclusions. First, the Si-to-PA flux is

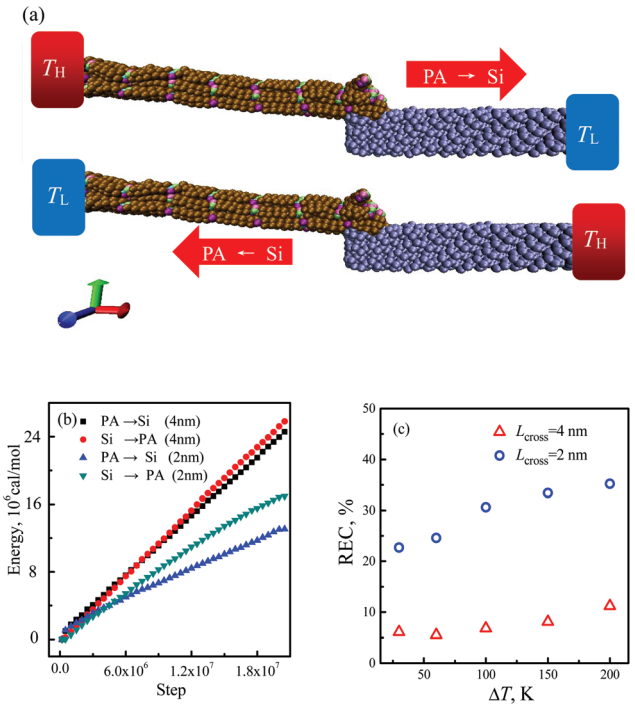

Fig. 5 (a) Schematic of the MD method for the PA/Si nanowires; (b) energy accumulation of the thermostats, ΔT = 100 K, L_{cross} is set as 2 nm and 4 nm; and (c) thermal rectification ratios varying with ΔT and L_{cross}.

always larger than the PA-to-Si flux. This agrees well with our experimental results. Second, the interfacial resistance increases as L_{cross} drops from 4 nm to 2 nm because the curve of the former is steeper than the latter. Third, the difference between the PA-to-Si and Si-to-PA fluxes is more significant when L_{cross} = 2 nm. This implies that shorter contact length leads to a higher thermal rectification ratio. Fig. 5c presents the thermal rectification ratios as a function of ΔT and L_{cross}. It shows that the decrease in L_{cross} and the increase of ΔT leads to the augmentation of the thermal rectification ratio. The former has a more significant effect on thermal rectification than the latter. *Versus* the experiments, the MD simulations show a clearer trend of the thermal rectification ratio, which is due to the much higher heat flux applied in the latter. In our experiments, the heat flux is about 0.1 MW m^{-2}, while in the MD simulations, it is usually higher than 10^3 MW m^{-2}.

We should emphasize that the conclusions of ref. 29 are completely different from ours although the authors likewise studied the thermal rectification of the organic/inorganic interface. They found that the heat transport from PE to Si has a higher thermal conductance. We note that they used periodic boundary conditions in all directions, *i.e.*, they nearly simulated bulk materials other than nanowires. The nanostructures usually possess extraordinary features *versus* bulk materials.[49,50] To confirm the difference between nanostructures and bulk materials, we also investigate the thermal rectification of the bulk PA/Si interface. Fig. 6a shows the schematic of the bulk PA/Si interface. The temperature profile is shown in Fig. 6b. The temperature difference of Si is far below that of PA suggesting that the thermal conductance of bulk Si is much larger than that of PA. Fig. 6c shows the energy accumulation of the PA-to-Si and Si-to-PA cases. The thermal rectification ratio is estimated based on the slopes of the two curves, namely, η = 1.42/0.81–1 = 75%. The PA-to-Si heat flux has a higher thermal conductance, and η can reach 75%. For bulk materials, the possible mechanism of thermal rectification is the dependence of thermal properties on space and temperature. The thermal conductivity of the polymer increases with increasing temperature (see the ESI, Note 4†), but it is reversed for Si.[43] Apparently, the PA-to-Si heat flux should have higher thermal conductance because PA is placed in the high temperature region and Si is in the low temperature region. It should be emphasized that for the bulk system, the thermal rectification is not due to the temperature-dependence of the interface thermal resistance, but due to the temperature-dependence of the thermal conductance. In other words, for PA/Si nanowires, the temperature-dependence of the thermal conductance will not improve but will actually suppress the thermal rectification effect. We estimate that the thermal rectification ratio will increase about 6% if temperature-dependence is excluded (see in the ESI, Note 5†). Generally, the PA/Si nanowire interface and its bulk counterpart have very different thermal rectification mechanisms due to the features of the nanostructures. Nanostructures have an extremely significant edge/surface effect leading to phonon lateral confinement. While phonons are the main energy carriers for heat conduction in crystals, the phonon lateral confinement has a strong impact on thermal properties. It is essential for the thermal rectification of homogeneous materials such as asymmetric graphene nanoribbons and non-uniform nanofilms.[6] First, we show how the phonon density of states (DOS) reveals how lateral confinement affects phonons. The phonon DOS is computed by taking the Fourier transform

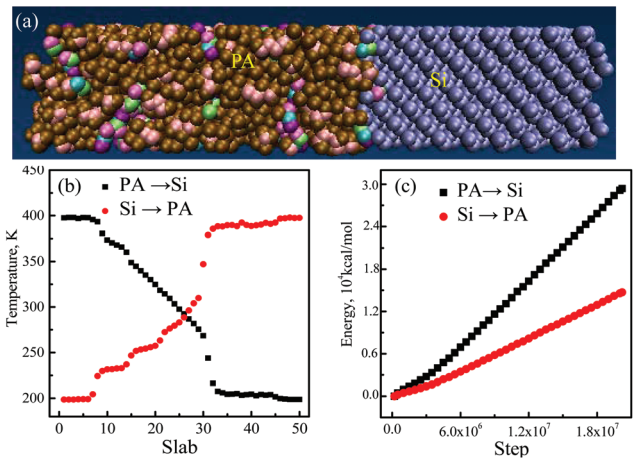

Fig. 6 (a) Schematic of the bulk PA/Si interface; (b) temperature profiles of PA and Si; and (c) energy accumulation of PA-to-Si and Si-to-PA cases.

This journal is © The Royal Society of Chemistry 2017

of the velocity autocorrelation function (VAF).[51] The VAF is expressed as

$$\mathrm{VAF}(t) = \langle v(0)\cdot v(t)\rangle = \left\langle \frac{1}{N}\sum_{i=1} v_i(0)\cdot v_i(t)\right\rangle, \quad (5)$$

where $v_i(t)$ denotes the velocity of atom i at time t. Fig. 7 shows the DOS of the atoms in PA and Si. PA has six types of atoms, and we merely focus on three typical types—nitrogen, oxygen and sp^2 carbon. For ease of description, the DOS of the edge atoms is called EDOS (edge DOS), otherwise, IDOS (interior DOS). The results show that the proportion of low frequency phonons in EDOS is higher than that in IDOS for all atom types. This suggests that the edge makes the phonon spectra shift to the low frequency region, and the peaks are weakened. Hence, the phonon localization occurs on the edge of the PA and the silicon nanowires. The phonon modes are softened, which means the thermal conductivity reduces.[52] So, the extent of phonon localization can reflect the relative value of the thermal conductivity. This localization is selective to certain modes.[6,53] Thus, the thermal rectification at the PA/Si nanowire interface is possibly due to the different extents of phonon localization for the different heat flux directions.

The extent of phonon localization can be qualitatively described by phonon spatial distribution. The distribution of a specific range, Λ, of phonon modes at atom i is

$$p_{\Lambda,i} = \frac{\int_{\Lambda} \mathrm{DOS}_i \mathrm{d}\omega}{\int_0^{\infty} \mathrm{DOS}_i \mathrm{d}\omega}. \quad (6)$$

Considering that Si is a monoatomic crystal, we use the phonon spatial distribution of the Si nanowire to visualize the phonon localization in the PA/Si interface. For bulk Si, the peak of DOS is about 16 THz, and we set Λ as 15 to 17 THz. Fig. 8 shows the phonon spatial distributions of the Si nanowire with PA-to-Si and Si-to-PA heat fluxes, which are calculated based on eqn (6). Three points should be mentioned for Fig. 8. First, $p_{\Lambda,i}$ of the edge atoms is different from that of the interior atoms, which implies that localized phonon modes exist at the edge, since there are few localized modes in interior atoms. Second, the atoms in Fig. 8a generally have higher $p_{\Lambda,i}$ than the atoms in Fig. 8b, especially for those close to the interface. This means that the localization extent of the Si-to-PA heat flux is less than that of the PA-to-Si heat flux. Third, the atoms in the internal domain are only affected to a minor degree. We can infer that the atoms in the interface play a dominant role in thermal rectification. Only at the nanoscale is the interfacial effect significant. Hence, this further demonstrates that the nanoscale is an essential condition for the interface-induced thermal rectification. In summary, the different phonon localization extent at the interface of PA/Si suggests that the Si-to-PA heat flux has higher thermal conductance than the PA-to-Si heat flux in PA/Si nanowires.

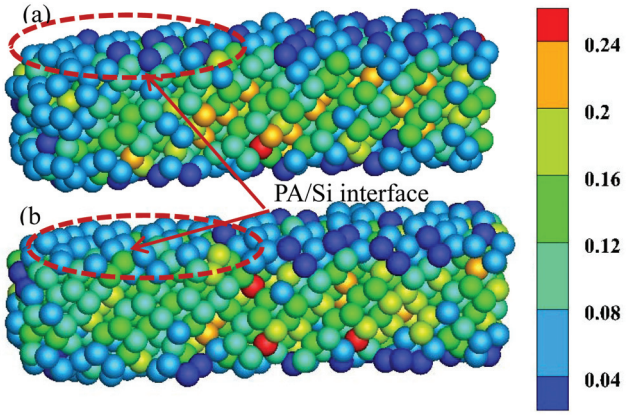

Fig. 8 Phonon (15 to 17 THz) spatial distribution of Si nanowire with (a) PA-to-Si and (b) Si-to-PA heat fluxes.

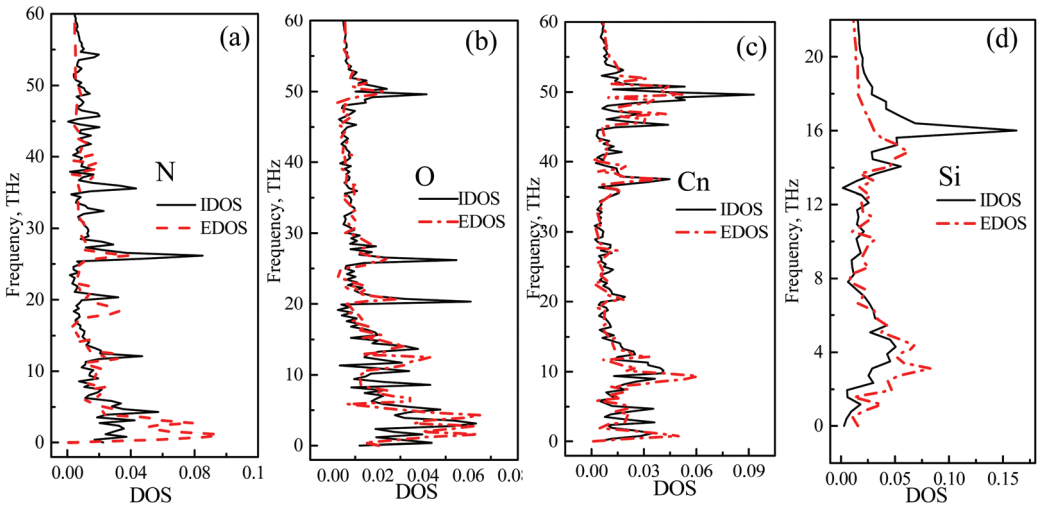

Fig. 7 DOS of interior and edge atoms. Atoms in PA (a) N: nitrogen, (b) O: oxygen, (c) Cn: sp^2 carbon, and (d) Si atom. Solid lines refer to interior atoms; dotted and dashed lines refer to edge atoms.

4. Conclusions

To summarize, we identified a thermal rectification effect in the PA/Si nanowire interface. Both the experimental results and the MD simulations suggested that the thermal conductance is higher when the heat flux is from Si to PA. The experiments resulted in a 2.7% to 3.5% thermal rectification ratio. The system temperature has a slight influence on the thermal rectification ratio, but the increase in the interfacial resistance or heat flux can lead to an increase in thermal rectification ratio. Interestingly, we find that the thermal rectification of the PA/Si nanowires is completely contrary to its bulk counterpart. In bulk PA/Si, the mechanism of thermal rectification depends on the thermal property change with space and temperature, but in PA/Si nanowires, the mechanism points to phonon localization. The phonon spatial distribution of the Si nanowire can be used to visualize the phonon localization in the PA/Si interface. This shows that the localized modes generally gather on the edge, and the localization extent of the PA-to-Si heat flux is larger than that of the Si-to-PA heat flux. Thus, the latter has a higher thermal conductance. Our work reveals the physical mechanism of thermal rectification caused by the interfacial effect at the nanoscale. It offers a guiding significance for the design of interface-based thermal rectifiers in the future.

Acknowledgements

This work is financially supported by the National Natural Science Foundation of China (No. 51676108, 51356001), the Science Fund for Creative Research Group (No. 51621062), and the Tsinghua National Laboratory for Information Science and Technology of China (TNList). We also would like to thank Dr Renkun Chen from the Department of Mechanical and Aerospace Engineering, University of California, San Diego, for offering support in the experiments.

References

1 N. Li, J. Ren, L. Wang, G. Zhang, P. Hänggi and B. Li, *Rev. Mod. Phys.*, 2012, **84**, 1045.
2 N. A. Roberts and D. G. Walker, *Int. J. Therm. Sci.*, 2011, **50**, 648–662.
3 N. Bender, J. D. Bodyfelt, H. Ramezani, D. N. Christodoulides, F. M. Ellis and T. Kottos, *Phys. Rev. Lett.*, 2013, **110**, 345.
4 B. Li, L. Wang and G. Casati, *Appl. Phys. Lett.*, 2006, **88**, 143501.
5 C. Starr, *Physics*, 1936, **7**, 15.
6 Y. Wang, A. Vallabhaneni, J. Hu, B. Qiu, Y. P. Chen and X. Ruan, *Nano Lett.*, 2014, **14**, 592.
7 L. Wang and B. Li, *Phys. Rev. Lett.*, 2008, **101**, 267203.
8 P. Ben-Abdallah and S. A. Biehs, *Appl. Phys. Lett.*, 2013, **101**, 191907.
9 M. Terraneo, M. Peyrard and G. Casati, *Phys. Rev. Lett.*, 2002, **88**, 094302.
10 Z. Liu and B. Li, *Phys. Rev. E: Stat. Phys., Plasmas, Fluids, Relat. Interdiscip. Top.*, 2007, **76**, 051118.
11 L. Wang and B. Li, *Phys. Rev. Lett.*, 2007, **99**, 177208.
12 Y. Li, X. Shen, Z. Wu, J. Huang, Y. Chen, Y. Ni and J. Huang, *Phys. Rev. Lett.*, 2015, **115**, 195503.
13 N. Yang, G. Zhang and B. Li, *Appl. Phys. Lett.*, 2009, **95**, 033107.
14 G. Wu and B. Li, *Phys. Rev. B: Condens. Matter*, 2007, **76**, 085424.
15 Y. Y. Liu, W. X. Zhou, L. M. Tang and K. Q. Chen, *Appl. Phys. Lett.*, 2014, **105**, 203111.
16 C. W. Chang, D. Okawa, A. Majumdar and A. Zettl, *Science*, 2006, **314**, 1121.
17 M. J. Martínezpérez, A. Fornieri and F. Giazotto, *Nat. Nanotechnol.*, 2015, **10**, 303.
18 J. Lee, V. Varshney, A. K. Roy, J. B. Ferguson and B. L. Farmer, *Nano Lett.*, 2012, **12**, 3491.
19 N. Yang, G. Zhang and B. Li, *Appl. Phys. Lett.*, 2008, **93**, 243111.
20 C. Dames, *J. Heat Transfer*, 2009, **131**, 177.
21 C. Y. Tso and C. Y. H. Chao, *Int. J. Heat Mass Transfer*, 2016, **93**, 605.
22 M. Hu, J. V. Goicochea, B. Michel and D. Poulikakos, *Appl. Phys. Lett.*, 2009, **95**, 151903.
23 Z. Chen, C. Wong, S. Lubner, S. Yee, J. Miller and W. Jang, *Nat. Commun.*, 2014, **5**, 5446.
24 C. R. Otey, W. T. Lau and S. Fan, *Phys. Rev. Lett.*, 2010, **104**, 154301.
25 X. Zhang, M. Hu and D. Tang, *J. Appl. Phys.*, 2013, **113**, 194307.
26 D. Seqal, *Phys. Rev. E: Stat. Phys., Plasmas, Fluids, Relat. Interdiscip. Top.*, 2009, **79**, 012103.
27 D. Seqal, *Phys. Rev. Lett.*, 2009, **100**, 105901.
28 H. Tian, D. Xie, Y. Yang, T. L. Ren, G. Zhang and Y. F. Wang, *Sci. Rep.*, 2012, **2**, 00523.
29 M. Hu, P. Keblinski and B. Li, *Appl. Phys. Lett.*, 2008, **92**, 211908.
30 S. Pal and I. K. Puri, *Nanotechnology*, 2014, **25**, 345401.
31 J. Zhu, K. Hippalgaonkar, S. Shen, K. Wang, Y. Abate and S. Lee, *Nano Lett.*, 2014, **14**, 4867.
32 A. L. Cottrill and M. S. Strano, *Adv. Energy Mater.*, 2015, **5**, 1500921.
33 R. Chen, Y. Cui, H. Tian, R. Yao, Z. Liu and Y. Shu, *Sci. Rep.*, 2015, **5**, 08884.
34 J. Maier, E. Scheer, P. Leiderer and M. Schmotz, *New J. Phys.*, 2011, **13**, 1367.
35 R. Xie, C. T. Bui, B. Varghese, Q. Zhang, C. H. Sow and B. Li, *Adv. Funct. Mater.*, 2011, **21**, 1602.
36 W. Xu, G. Zhang and B. Li, *J. Appl. Phys.*, 2014, **116**, 134303.
37 R. Rurali, X. Cartoixà and L. Colombo, *Phys. Rev. B: Condens. Matter*, 2014, **90**, 041408.
38 J. Ren and J. X. Zhu, *Phys. Rev. B: Condens. Matter*, 2013, **8**, 291.
39 J. Wang and Z. Zheng, *Phys. Rev. E: Stat. Phys., Plasmas, Fluids, Relat. Interdiscip. Top.*, 2010, **81**, 95.

 This journal is © The Royal Society of Chemistry 2017

40 T. Zhang and T. Luo, *Small*, 2015, **11**, 4656.
41 J. Zheng, M. C. Wingert, E. Dechaumphai and R. Chen, *Rev. Sci. Instrum.*, 2013, **84**, 114901.
42 Z. Zhong, M. C. Wingert, J. Strzalka, H. H. Wang, T. Sun and J. Wang, *Nanoscale*, 2014, **6**, 8283.
43 R. Chen, A. I. Hochbaum, P. Murphy, J. Moore, P. Yang and A. Majumdar, *Phys. Rev. Lett.*, 2008, **101**, 105501.
44 S. Plimpton, *J. Comput. Phys.*, 1995, **117**, 1.
45 H. J. C. Berendsen, J. P. M. Postma, W. F. V. Gunsteren, A. Dinola and J. R. Haak, *J. Chem. Phys.*, 1984, **81**, 3684.
46 S. Goudeau, M. Charlot, C. Vergelati and F. Müller-Plathe, *Macromolecules*, 2004, **37**, 8072.
47 J. W. Caldwell and P. A. Kollman, *J. Phys. Chem.*, 1995, **99**, 6208.
48 F. H. Stillinger and T. A. Weber, *Phys. Rev. B: Condens. Matter*, 1985, **31**, 5262.
49 S. Volz, *Microscale and Nanoscale Heat Transfer*, Springer, 2007.
50 D. G. Cahill, W. K. Ford, K. E. Goodson and G. D. Mahan, *J. Appl. Phys.*, 2003, **93**, 793.
51 G. J. Hu and B. Y. Cao, *Mol. Simul.*, 2012, **38**, 823.
52 Q. X. Pei, Z. D. Sha and Y. W. Zhang, *Carbon*, 2011, **49**, 4752–4759.
53 A. Bodapati, P. K. Schelling, S. R. Phillpot and P. Keblinski, *Phys. Rev. B: Condens. Matter*, 2006, **74**, 4070.

This journal is © The Royal Society of Chemistry 2017